AD-A063 564 ROCKWELL INTERNATIONAL THOUSAND OAKS CALIF SCIENCE --ETC F/G 20/4
AN INVISCID MODEL FOR SUBMERGED TRANSONIC WALL JETS,(U)
DEC 76 N D MALMUTH, W D MURPHY N00014-76-C-0350
UNCLASSIFIED SCPP-76-124 NL

| OF |
ADA
063564

END
DATE
FILMED
3 -79
DDC

77-174

An Inviscid Model for Submerged Transonic Wall Jets

N.D. Malmuth and W.D. Murphy, *Rockwell International, Thousand Oaks, Ca.*

AIAA 15th AEROSPACE SCIENCES MEETING

Los Angeles, Calif./January 24-26, 1977

AN INVISCID MODEL FOR SUBMERGED TRANSONIC WALL JETS

N. D. Malmuth* and W. D. Murphy†
Rockwell International, Science Center
Thousand Oaks, California 91360

Abstract

Nonlinear flow phenomena in transonic wall jets prototypic of propulsive lift devices such as lifting ejector augmenters and upper surface blown wings have been studied using the Karman-Guderley model. From modern line relaxation methods, an efficient computational method has been developed to treat the diversity of shock patterns produced by various wall shapes and exit conditions. Associated with the algorithm is a far field determined analytically from the boundary value problem appropriate to subsonic conditions far downstream. Numerical results for circular arc boattails indicate rapid relaxation of the wall induced disturbances, even in the supersonic region. Partially subsonic and supersonic jet exit conditions lead to the anticipated wave interactions. Studies of other shapes show that branch point singular behavior associated with satisfaction of a Kutta condition at the wall trailing edge is obtained by demanding continuity of the perturbation potential at this point.

Introduction

Increased emphasis on propulsive lift devices in tactical and advanced aircraft has stressed the need for greater understanding of the underlying fluid dynamic processes which control the degree of force augmentation that can be achieved. Such concepts are exemplified in recently proposed supercritical jet flap implementations for advanced highly maneuverable aircraft such as the NASA HiMAT. Similar mechanisms are illustrated in upper surface blowing configurations and lifting ejector augmenters which are embodied in the Navy's XFV-12A.[1] An essential element in the operation of these devices are Coanda-type wall jets consisting of jets bounded by curved walls in which a transonic primary flow entrains an ambient secondary stream through turbulent mixing processes. Existing models for such wall jets stress the incompressible treatment of these phenomena using eddy viscosity and energy methods. Correspondingly, there is a need for simulations that include the effects of nonlinearities, mixed flow, and wave interactions on the development of the wall pressure distributions and overall augmentation forces.

Previous investigations of related phenomena are limited to the treatment of inviscid shockless free jets, and include the work of Chaplygin,[2] Frankl,[3] and Guderley[4] all of which employ hodograph methods. To study shock development and mixed flow phenomena, we have applied modern relaxation methods to treat arbitrary jet exit velocity distributions and assess the influence of an adjacent wall boundary.

In this paper, the computational model will be discussed from analytical and numerical viewpoints. In analogy to unbounded cases such as airfoil flows, the far field is employed to condition the numerical problem and provide useful information about the decay of disturbances. Both free and wall jets are discussed for several examples illustrating various features of this class of flows.

Formulation

Referring to the physical configuration depicted in Fig. 1, a jet is shown exhausting from the exit OC bounded by the wall OQ and a mixing layer which has been idealized as the slip line CB. This approximation neglects turbulent diffusion processes in the study of wave interactions with the shear layer, but these phenomena can be incorporated in later refinements. Furthermore, it will be assumed that wall and jet turning angles are small. In contrast to the usual jet formulations, in which an upstream cowl shape is specified, or stagnation conditions are assumed,[2-6] this analysis will treat a specified exit Mach number distribution. Additional assumptions are irrotationality and subsonic conditions infinitely far downstream. The methods applied here can be generalized to cases where these restrictions are not present. Finite length walls OQ are considered in keeping with relevance to upper surface blown wings and other propulsive lift devices.

Returning to Fig. 1, the equations of slip lines $S_1(x,y)$, $S_2(x,y)$, and the wall boundary $B(x,y)$ are assumed as

$$\text{CB:}\quad S_1 = y - d - \delta G_1(x) = 0$$

$$\text{QA:}\quad S_2 = y - \delta G_2(x) = 0$$

$$\text{OQ:}\quad B = y - \delta f(x) = 0$$

where δ is a characteristic flow deflection parameter. In a small disturbance limit in which the scaled jet exit height $D \equiv d\delta^{1/3}$, the wall length length L, and the transonic similarity parameter $K = (1 - M_\infty^2)/\delta^{2/3}$ are held fixed, as $\delta \to 0$, the asymptotic expansions of the velocity, pressure P, and density ρ are

$$\frac{\vec{q}}{U}(x,y;M_\infty,\delta,d,L) \doteq \left[1 + \delta^{2/3}\phi_x(x,Y;K,D,L) + \ldots\right]\vec{i} + \left[\delta\phi_Y + \ldots\right]\vec{j} \qquad (1.1a)$$

$$P/P_\infty \doteq 1 - \gamma\delta^{2/3}\phi_x + \ldots \qquad (1.1b)$$

$$\rho/\rho_\infty \doteq 1 + \delta^{2/3}\sigma + \ldots \qquad (1.1c)$$

where the subscript ∞ signifies conditions at $x = \infty$, ϕ is the perturbation potential, P_∞ is the ambient pressure, $U = a_\infty M_\infty$, $a_\infty^2 = \gamma P_\infty/\rho_\infty$, ρ_∞

*Project Manager, Fluid Dynamics Research; Associate Fellow, AIAA
†Member of Technical Staff, Mathematical Sciences Group

is the density, a_∞ is the speed of sound, $\vec{q}$ is the flow velocity and the scaled coordinate $Y = \delta^{1/3} y$ is also fixed in the limit. If a further transformation is introduced in which $\tilde{y} = \sqrt{K}\, Y$, a boundary value problem can be formulated for the case of an elliptic far field. The region can be considered as the rectangular domain shown in Fig. 2, corresponding to transfers of the boundary conditions to the appropriate undisturbed streamlines allowed by the small disturbance limit. Dropping the tildes, the following small disturbance equation holds inside OQABCO

$$\Delta\phi \equiv \left(\partial^2/\partial x^2 + \partial^2/\partial y^2\right)\phi = (\gamma+1)\left(\partial u^2/\partial x\right)/2K \quad , \quad (u \equiv \phi_x) \tag{1.2}$$

where we define functions $\bar{u}$ and Φ such that

$$u(x,y) = \bar{u}(x,Y)$$

$$\phi(x,y) = \Phi(x,Y) \quad .$$

Invoking continuity of pressure and flow tangency along the slip lines, we have, with $a \equiv D\sqrt{K}$

$$\phi(x,a) = 0 \tag{1.3a}$$

$$\phi_y(x,a) = G_1'(x) \quad , \quad 0 \le x \le \infty \tag{1.3b}$$

$$\phi(x,0) = C_1 \quad , \quad L \le x \le \infty \tag{1.3c}$$

$$\phi_y(x,0) = G_2'(x) \quad , \quad L \le x \le \infty \tag{1.3d}$$

where the constant C_1 is to be computed by iteration. In this approximation, the slip lines are therefore not truly free, the unknown functions G_i' being computed from the solution by a simple differentiation. The remaining boundary conditions are

$$\phi_y(x,0) = f'(x) \equiv F(x) \quad , \quad 0 \le x \le L \tag{1.3e}$$

$$\phi_x(0,y) = h(y) = H(Y) \tag{1.3f}$$

Equation (1.3f) is representative of the initial exit velocity profile which conceivably is determined by the upstream duct contour and stagnation pressure.

Far Field

To complete the formulation of the problem for subsonic conditions far downstream, the asymptotic behavior is derived in this section. Introducing a Green's function G satisfying homogeneous Dirichlet conditions on OA and CB, and homogeneous Neumann conditions on OC and AB in Fig. 2 with

$$\Delta G = \delta(P,Q) \equiv \delta(x-\xi)\delta(y-\eta)$$

where $Q(\xi,\eta)$ is the source point and P is the field point, Green's theorem applied to the region OQABCO gives the following integrodifferential equation for ϕ

$$\phi = \sum_{i=1}^{4} I_i$$

where

$$I_1 = \frac{\gamma+1}{2K} \int_0^\infty d\xi \int_0^a G(x,y;\xi,\eta)\left(\partial u^2/\partial\xi\right)d\eta$$

$$I_2 = -\int_0^L \phi(\xi,0)\, \frac{\partial G}{\partial \eta}\,(x,y;\xi,0)\,d\xi$$

$$I_3 = -C_1 \int_L^\infty \frac{\partial G}{\partial \eta}\,(x,y;\xi,0)\,d\xi$$

$$I_4 = \int_0^a h(\eta) G(x,y;0,\eta)\,d\eta$$

The quantity G may be obtained from the cosine transform where

$$\bar{G} = \int_0^\infty G \cos px\,dx$$

$$G = \frac{2}{\pi} \int_0^\infty \bar{G} \cos px\,dp$$

The subsidiary equations for $\bar{G}$ are

$$\frac{d^2\bar{G}}{dy^2} - p^2\bar{G} = \delta(y-\eta)\cos p\xi$$

$$\Rightarrow \left[\frac{d\bar{G}}{dy}\right]_{y=\eta} \equiv \left(\frac{d\bar{G}}{dy}\right)_{y=\eta+} - \left(\frac{d\bar{G}}{dy}\right)_{y=\eta-} = \cos p\xi$$

$$[\bar{G}]_{y=\eta} \equiv (G)_{y=\eta+} - (G)_{y=\eta-} = 0$$

$$\bar{G}(p,0;\xi,\eta) = \bar{G}(p,a;\xi,\eta) = 0$$

Implying that

$$\bar{G} = \frac{\sinh p(\eta-a)\, \sinh py\, \cos p\xi}{p \sinh pa} \quad , \quad y < \eta \tag{1.4a}$$

$$= \frac{\sinh p\eta\, \sinh p(y-a)\, \cos p\xi}{p \sinh pa} \quad , \quad y > \eta \tag{1.4b}$$

Equations (1.4) can be inverted by a treatment of appropriate contour versions for the inversion integrals, initially, without the $\cos p\xi$ factor and, subsequently, including it using the shift theorem. To obtain convergence and exponential decay of the integrand, the appropriate closure for the contour is a large semicircle $|p| = R$, $R \to \infty$, with $\mathrm{Im}\, p \gtrless 0$ for $x \gtrless 0$. Summing the residues at the poles $p = n\pi i$, $n = (\mathrm{sgn}\, x)(1,2,3,\ldots)$, gives the following final expression for G:

$$-\pi G = \sum_1^\infty n^{-1}\sin n\alpha y \sin n\alpha\eta\left\{e^{-n\alpha(x+\xi)} + e^{-n\alpha|x-\xi|}\right\} \qquad (1.5)$$

$$\alpha \equiv \pi/a$$

Equation (1.5) is valid for $y \gtrless \eta$, $x \gtrless \xi$, and can be summed as the integral of a geometric series giving

$$-2\pi G = S\left(\alpha(x+\xi),\alpha(\eta+y)\right) + S\left(\alpha(x+\xi),\alpha(\eta-y)\right) - S\left(\alpha|x-\xi|,\alpha(\eta+y)\right) - S\left(\alpha|x-\xi|\ \alpha(\eta-y)\right)$$

$$\Rightarrow G = \frac{1}{4\pi}\,\ell n\left\{\left[\frac{1-\cos\alpha(\eta-y)\operatorname{sech}\alpha(x+\xi)}{1-\cos\alpha(\eta+y)\operatorname{sech}\alpha(x+\xi)}\right] \times \left[\frac{1-\cos\alpha(\eta-y)\operatorname{sech}\alpha|x-\xi|}{1-\cos\alpha(\eta+y)\operatorname{sech}\alpha|x-\xi|}\right]\right\} \qquad (1.5')$$

where

$$S(A,B) \equiv \sum_1^\infty n^{-1}e^{-nA}\cos nB = -\ell n|1-e^{-Z}|$$

$$= -\frac{1}{2}\,\ell n\left(1-2e^{-A}\cos B + e^{-2A}\right)$$

$$Z \equiv A + iB$$

An inspection of these formulas reveals that G is exponentially small as $x \to \infty$, and is logarithmically singular at the source point as anticipated.

Based on (1.5), the dominant term of the asymptotic expansion of I_1 as $x \to \infty$ is given by the formula

$$I_1 \doteq \frac{\gamma+1}{aK}\,e^{-\alpha x}\sin\alpha y \int_0^a \sin\alpha n\,dn \int_0^x u^2\sinh\alpha\xi\,d\xi \qquad (1.6)$$

where in the evaluation,* the contribution of the simple pole of G_ξ vanishes, and integrals of the form

$$\int_0^a dn \int_0^\infty e^{-\alpha|x-\xi|}f(\xi,n)\,d\xi \quad \text{and}$$

$$\int_0^a dn \int_0^\infty e^{-\alpha(x+\xi)}f(\xi,n)\,d\xi \qquad (1.7)$$

arise. The multiplication by u^2 of the asymptotic expansion represented by (1.5) as $x \to \infty$ and its subsequent integration with respect to ξ formally gives a development dominated by these integrals. Writing the inner integral of the first of (1.7), as

$$\int_0^\infty e^{-\alpha|x-\xi|}f(\xi,n)\,d\xi = e^{-\alpha x}\int_0^x e^{\alpha\xi}f(\xi,n)\,d\xi + e^{\alpha x}\int_x^\infty e^{-\alpha\xi}f(\xi,n)\,d\xi \quad ,$$

and if the $e^{-\alpha x}$ factor of the first integral on the left-hand side is indicative of the behavior of ϕ as $x \to \infty$, then u^2 and f are $O(e^{-2\alpha\xi})$ in this limit. If u^2 and f are bounded on the range of integration, the first integral converges and the second is $O(e^{-2\alpha x})$ as $x \to \infty$. The second integral in (1.7) requires no such decomposition and is also convergent; hence, (1.6) follows. Evaluating the remaining integrals, using (1.5) and (1.5'), the final expression for the far-field is

$$\Phi \doteq \Phi_{FF} = C_1(1-Y^*) + C_{FF}e^{-x^*}\sin\pi Y^* + O(e^{-2x^*}) \quad \text{as} \quad x \to \infty \qquad (1.8a)$$

where

$$C_{FF} \equiv \frac{\gamma+1}{DK}\int_0^D \sin\pi Y^*dY \int_0^\infty \phi_x^2(\xi,Y)\sinh\xi^*d\xi - \frac{2\sqrt{K}}{\pi}\int_0^D H(Y)\sin\pi Y^*dY + \frac{2}{D\sqrt{K}}\int_0^L \Phi(\xi,0)\cosh\xi^*d\xi - 2C_1\sinh L^* \qquad (1.8b)$$

$$x^* \equiv \pi x/D\sqrt{K} \quad , \quad \xi^* \equiv \pi\xi/D\sqrt{K} \quad , \quad L^* \equiv \pi L/D\sqrt{K} \quad ,$$

$$Y^* \equiv Y/D \quad .$$

Numerical Analysis

The numerical procedure is similar to that one first developed by Murman[7] and extended by Jameson[8] and Bailey and Ballhaus.[9] Briefly, the transonic potential equation in divergence form is discretized using central differences when the equation is elliptic and backward differences when it is hyperbolic. Thus, we may write

$$\left(K\Phi_x - \frac{\gamma+1}{2}\Phi_x^2\right)_x + \left(\Phi_Y\right)_Y \approx (1-\mu_i)\left\{K(\Phi_{xi+1/2}-\Phi_{xi-1/2}) - \frac{\gamma+1}{2}(\Phi^2_{xi+1/2}-\Phi^2_{xi-1/2})\right\}/P_i + \mu_{i-1}\left\{K(\Phi_{xi-1/2}-\Phi_{xi-3/2}) - \frac{\gamma+1}{2}(\Phi^2_{xi-1/2}-\Phi^2_{xi-3/2})\right\}/P_i + (\Phi_{Yj+1/2} - \Phi_{Yj-1/2})/q_j \qquad (2.1)$$

*The upper limit of the inner integral can be interpreted as ∞ to within terms of higher order involving $e^{-\alpha x}$ as $x \to \infty$. This interpretation is made in Eq. (1.8).

$$\approx (1-\mu_i)\left[K - \frac{\gamma+1}{2}\left(\frac{\Phi_{i+1}-\Phi_i}{p_{i+1/2}} + \frac{\Phi_i-\Phi_{i-1}}{p_{i-1/2}}\right)\right]$$

$$\times\left[\frac{\Phi_{i+1}-\Phi^+_i}{p_{i+1/2}p_i} - \frac{\Phi^+_i-\Phi^+_{i-1}}{p_i p_{i-1/2}}\right]$$

$$+ \mu_{i-1}\left[K - \frac{\gamma+1}{2}\left(\frac{\Phi_i-\Phi_{i-1}}{p_{i-1/2}} + \frac{\Phi_{i-1}-\Phi_{i-2}}{p_{i-3/2}}\right)\right]$$

$$\times\left[\frac{\Phi^*_i-\Phi^+_{i-1}}{p_{i-1/2}p_i} - \frac{\Phi^+_{i-1}-\Phi_{i-2}}{p_i p_{i-3/2}}\right] + \frac{\Phi^+_{j+1}-\Phi^+_j}{q_j q_{j+1/2}} - \frac{\Phi^+_j-\Phi^+_{j-1}}{q_j q_{j-1/2}} \qquad (2.2)$$

where the missing subscript is j when only i's are present and i when only j's are present. For example, $\Phi_{i-1} \equiv \Phi_{i-1,j}$ and $\Phi_{j+1} \equiv \Phi_{i,j+1}$. Also,

$$p_i = (x_{i+1} - x_{i-1})/2 \qquad q_j = (Y_{j+1} - Y_{j-1})/2$$

$$p_{i-3/2} = x_{i-1} - x_{i-2} \qquad q_{j-1/2} = Y_j - Y_{j-1}$$

$$p_{i-1/2} = x_i - x_{i-1} \qquad q_{j+1/2} = Y_{i+1} - Y_j$$

$$p_{i+1/2} = x_{i+1} - x_i$$

and

$$\mu_i = \begin{cases} 0 & \text{if the point } (x_i, Y_j) \text{ is elliptic} \\ 1 & \text{if the point } (x_i, Y_j) \text{ is hyperbolic} \end{cases}$$

Define

$$VC_i \equiv K - \frac{\gamma+1}{2}\left(\frac{\Phi_{i+1} - \Phi_i}{p_{i+1/2}} + \frac{\Phi_i - \Phi_{i-1}}{p_{i-1/2}}\right).$$

then

$$\mu_i = \begin{cases} 0 & \text{if } VC_i \geq 0 \\ 1 & \text{if } VC_i < 0 \end{cases}.$$

Here, the iterations are viewed as steps in pseudo-time with Φ^+ (NEW) and Φ (old) values. In addition,

$$\frac{\Phi^*_i}{p_{i-1/2}p_i} \equiv \Phi^+_i\left(\frac{1}{p_i p_{i-1/2}} + \frac{1}{p_i p_{i-3/2}}\right) - \Phi_i\left(\frac{1}{p_i p_{i-3/2}}\right)$$

These definitions guarantee that the linearized difference algorithm satisfies the von Neumann stability criterion. See Jameson[8] for the proof.

Overrelaxation is employed in the elliptic region ($\mu_{i,j} = \mu_{i-1,j} = 0$) only. First, define

$$e_1 \equiv 1/p_i p_{i-1/2} \quad , \quad e_3 \equiv 1/p_i p_{i+1/2} \quad ,$$

and

$$e_2 \equiv e_1 + e_3 \quad .$$

Then, the elliptic difference expression in Eq. (2.2) given by

$$\left[\frac{\Phi_{i+1}-\Phi^+_i}{p_{i+1/2}p_i} - \frac{\Phi^+_i-\Phi^+_{i-1}}{p_i p_{i-1/2}}\right] = e_1\Phi^+_{i-1} - e_2\Phi^+_i + e_3\Phi_{i+1}$$

is replaced by

$$e_1\Phi^+_{i-1} - \Phi^+_i e_2/\omega - \Phi_i e_2(1-1/\omega) + e_3\Phi_{i+1}$$

where ω is the overrelaxation parameter; i.e., $1 \leq \omega < 2$. Note that if $\omega = 1$, there is no change between the two expressions.

To improve stability near the sonic points, especially if a discontinuous wall boundary condition is being considered, it was found necessary, as in Bailey and Ballhaus,[9] to add to Eq. (2.1) the term

$$\frac{\varepsilon\Delta t}{x_i - x_{i-1}}\Phi_{xt} = \varepsilon\frac{(\Phi^+_i - \Phi_i) - (\Phi^+_{i-1} - \Phi_{i-1})}{(x_i - x_{i-1})^2}$$

where ε is chosen to be in the range $0 \leq \varepsilon \leq .5$.

Boundary Conditions

The boundary conditions $\Phi(x,D) = 0$ and $\Phi_y(x,0) = f'(x)$ may be incorporated into the numerical scheme using the same techniques described in Murman and Cole.[10] First, we shall concentrate on discussing the boundary condition at the jet exit $x = 0$, which may be of one of two types: (A) subsonic at the jet exit, and (b) partially or completely supersonic at the jet exit. The far field boundary condition will be treated later.

(A) Subsonic at the Jet Exit

Here the boundary condition is

$$\Phi_x(0,Y) = H(Y) \qquad 0 \leq Y \leq D$$

where

$$K - (\gamma+1)H(Y) > 0 \quad \text{for} \quad 0 \leq Y \leq D \quad .$$

In this case, we let $x_{1/2} = 0$, $x_1 - x_{1/2} = \Delta x/2$, $\mu_0 = 0$, and $\mu_1 = 0$, and we require $x_2 - x_1 = \Delta x$. Then, the x derivatives in Eqs. (2.1) and (2.2) become

$$\left[K(\phi_{x3/2} - \phi_{x1/2}) - \frac{\gamma+1}{2}(\phi^2_{x3/2} - \phi^2_{x1/2})\right]\Big/\Delta x$$

$$= \left[K - \frac{\gamma+1}{2}(\phi_{x3/2} + \phi_{x1/2})\right]\left[\phi_{x3/2} - \phi_{x1/2}\right]\Big/\Delta x$$

$$= \left[K - \frac{\gamma+1}{2}\left(\frac{\phi_2-\phi_1}{\Delta x} + H(Y)\right)\right]\left[\frac{\phi_2-\phi_1}{\Delta x} - H(Y)\right]\Big/\Delta x$$

(B) Partially or Completely Supersonic at the Jet Exit

For this case, two boundary conditions are required at $x = 0$; namely,

$$\phi_x(0,Y) = H(Y) \qquad 0 \leq Y \leq D$$

and

$$\phi(0,Y) = g(Y) \quad \text{for} \quad Y \in [0,D]$$

where

$$K - (\gamma+1)H(Y) < 0 \ .$$

For all points $Y \in [0,D]$ in which $K - (\gamma+1)H(Y) > 0$, $g(Y)$ need not exist.

If a point (x_1,Y_j) is elliptic, we use the discretization given in case (A). On the other hand, if (x_1,Y_j) is hyperbolic, we assume the grid may be extended to the left by $\Delta x/2$, and we let $x_0 = 0$, $x_{-1} = -\Delta x/2$, and $\phi_{0j} = \phi(0,Y_j) = g(Y_j)$.

Using Taylor's theorem,

$$\phi_{-1,j} = \phi_{0j} - \Delta x\phi_x(0,Y_j)/2 = g(Y_j) - \Delta x H(Y_j)/2$$

These values for ϕ_{0j} and $\phi_{-1,j}$ may now be substituted into Eq. (2.2) in the normal way, and line relaxation may be applied to the first column of unknowns along $x = x_1$.

The far field boundary condition given by Eq. (1.8) contains two unknown constants, C_1 and C_{FF}, which must be determined in an iterative fashion. The basic technique holds C_{FF} fixed while C_1 changes until the solution converges. Then, C_{FF} is updated by evaluating the integrals in Eq. (1.8b), and the procedure is repeated until C_{FF} also converges. In order to determine C_1, the mesh network is swept from left to right using line relaxation. After the potential is computed on the line $x = L$, extrapolation of the interior points yields $\phi(L,0) \equiv \phi_L$. Assuming only that ϕ is continuous at $x = L$, we set $C_1 = \phi(L,0) = \phi(x,0)$ for $x > L$, which guarantees that $\phi_x(x,0) = 0$ for $x > L$.

Singular Behavior Near Wall Trailing Edge

It is physically plausible that a Kutta condition given by

$$\phi_x(L-,0) = \phi_x(L+,0) = 0 \qquad (3)$$

is satisfied by the solution for trailing edge neighborhoods in unmixed flow. Because of (3), the nonlinear term in (1.2) can be assumed negligible, and ϕ is locally harmonic in the scaled variables. Let

$$z = x^* + iy \ , \quad x^* = x - L$$

$$\theta \equiv \arg z \ , \quad r \equiv \mathrm{mod}\ z$$

$$w(z) = u(x^*,y) - iv(x^*,y) = \text{complex velocity}$$

where

$$u = \phi_{x^*} \ , \quad v = \phi_y \ .$$

Then if the boundary conditions are locally linearized near the point $z = 0$, we obtain

$$v(x^*,0) \to F(L) \equiv \omega \ , \quad x^* \uparrow 0 \qquad (4a)$$

$$u(x^*,0) = 0 \ , \quad x^* > 0 \qquad (4b)$$

To dominant order, a sufficient condition to satisfy (3) and (4) near the origin is that w has the following branch point behavior

$$w = i(\omega + B\sqrt{z}) \quad \text{as} \quad z \to 0 \ , \quad (0 \leq \theta \leq \pi) \qquad (5)$$

where B is a real constant to be determined by matching with the outer nonlinear solution. Equation (5) implies that

$$\phi - \phi_L \doteq -\omega y - \frac{2}{3} Br^{3/2}\sin 3\theta/2 \qquad (6)$$

Several examples to be discussed indicate that the approach described previously in which ϕ is maintained continuous at the wall trailing edge gives numerical solutions that satisfy the Kutta condition (3). However, a rigorous proof that this is an implication of the algorithm has not been attempted. A similar procedure has been used by Krupp[11] to satisfy the Kutta condition in the solution of the transonic small disturbance lifting airfoil problem.

Results and Discussion

In addition to the assumptions given in the Introduction, the analysis previously described is not directly applicable to choked flows where upstream and downstream conditions are decoupled. Sonic zones comprising the entire vertical dimension of the flow field are thereby excluded. However, the foregoing methods can be extended to handle such cases.

A number of examples will now be considered. For these cases, the associated wall displacement

functions, and exit velocity distributions H(Y) are given in Table 1. For these cases, K is unity and D will take on this value for the remainder of this paper.

Table 1. Wall Jet Cases

Case	f = Wall Shape Function	H(Y)	Remarks
1	$f = f_1 = 0$, $0 \le x \le 1$ $= -(1-x)^2$, $1 \le x \le 2$ $= 3-2x$, $2 \le x \le L$	.075 $0 \le Y \le 1$	L = 3.8 for this and all other cases
2	$f = f_2 = -f_1$	↓	
3	$f = f_3 = 0$, $0 \le x \le 1$ $= [x^2-1+2(L+1)(1-x)]/2L$, $1 \le x \le L$	↓	Has discontinuous slope at x = 1
4	$f = f_4 = 0$, $0 \le x \le 1$ $= \frac{10(L-1)}{L\pi}\left\{\cos\frac{\pi(x-1)}{L-1}-1\right\}$, $1 \le x \le L$	↓	Has reflex curvature on curved ramp portion
5	$f = f_5 = -x^2$, $0 \le x \le 1$ $= 1-2x$, $1 \le x \le 2$ $= -3$, $2 \le x \le L$	h = 1 $0 \le Y \le 1/2$ = 0 , $1/2 \le Y \le 1$	$\phi = 0.2$ on $0 \le Y \le 1/2$

Wall pressure distributions for the convex ramp comprising Case 1 are shown in Fig. 3 for K = 1 and K = 1.46. Interpreting these results as those for different final M_∞'s downstream but with the same δ, the decrease in M_∞ leads to upstream motion of the terminating shock but a preservation of the shock strength. There is a smooth acceleration to critical conditions with the location of the sonic line established at the curvature discontinuity, x = 1. These calculations, which are typical of the other cases, cost approximately $60 on the Berkeley 7600 and ran 15-30 CP seconds. Figure 4 shows a close-up of the pressures near the trailing edge. The dashed line has a slope proportional to $\sqrt{x^*}$ appropriate to the singular behavior given by Eqs. (5) and (6) and the Kutta condition (3). Isobars shown in Fig. 5 are consistent with these remarks, and demonstrate the satisfaction of homogeneous pressure boundary conditions on the slip lines. Because of the weakness of the singularity, e.g., $\phi_{xx} \sim r^{-1/2}$ as $r \to 0$, special numerical treatments such as those of Woods[12] were not used.

In Figs. 6 and 7, rapid decay of the disturbances is indicated. The relaxation length for this decay from (1.8b) with D = K = 1, is π. This exponential decay is typical of flows confined by jet boundaries and is much more potent than for bodies in unbounded fields. Qualitatively similar effects have been discussed by Murman,[13] and Pinzola and Lo[14] in connection with tunnel wall interference on transonic airfoils. The distinction between confined and unconfined flows can be appreciated by an interpretation of the exponential series due to (1.5) arising in the far field developments dominated by (1.8). Because of linearity of the far field, this series is directly related to expansions occurring in analogous incompressible flow problems in which a singularity is reflected between free pressure boundaries yielding an image development in which the strengths alternate in sign to satisfy the slip line condition.* Thus, the relaxation to uniform conditions downstream which must be consistent with homogeneous conditions on the slip lines produces a more rapid decay than found in unconfined flows.

In Figs. 8a and 8b, the upper and lower slip lines obtained from integration of (1.3b) and (1.3d) are given for Case 1. It is evident from Fig. 8a that the curved surface in this approximation turns the flow so that the streams are parallel for $x \to \infty$. In the near field, it is evident from Fig. 8b that this is not quite the case. Asymptotic parallelism can be established for subsonic conditions far downstream by integration of the small disturbance continuity equation. Thus

$$G_1'(x) - G_2'(x) = \frac{d}{dx}\int_0^1 \left(Ku(x,Y) - \frac{Y+1}{2}u^2\right)dY \qquad (7)$$

and since $u = O(e^{-x^*})$, this expression shows that $G_1'(x) \to G_2'(x)$ as $x \to \infty$. Equation (7) can also be obtained by differentiating (1.8a) with respect to Y and using (1.3b) and (1.3d). For the case of a free jet with a symmetrical exit Mach number profile function H, i.e., H(Y-1/2) = H(1/2-Y), $G_1 = -G_2$ and the divergence theorem or integration of (7) between x = 0 and ∞ gives the displacement of the jet infinitely downstream as

$$G_1(\infty) = \frac{1}{2}\int_0^1 \left[KH(Y) - \frac{Y+1}{2}H^2\right]dY \qquad (8)$$

* Such a series can be summed by recognizing that it is a partial fraction expansion of a hyperbolic function which is exponentially small as $x \to \infty$, consistent with developments such as (1.8a).

where $G_1(0) = 0$ has been used.

Insight into the mechanisms causing acceleration to supercriticality can be obtained from the flow direction field for Case 1 shown in Fig. 9. For clarity, all isocline slopes have been magnified by a factor of 100, and only the entrance section $0 \leq x \leq 1$ is depicted. The expansion around the curved ramp on the interval $1 \leq x \leq 2$, leads to upstream influence in the subsonic region which turns most of the flow downward upstream of $x = 1$, producing throats and acceleration due to the stream tube contraction required by the zero slope boundary condition in that region. Also indicated is the "ballooning" due to the singularity occurring at (0,1), the top point of the jet exit station. In contradistinction to the trailing edge where $u \to 0$, local linearization cannot be used to characterize the flow behavior in this region, and some local similarity solution must be sought, presumably of the form $\phi = x^{\alpha} f(y/x^{\beta})$ where α and β are exponents to be determined.

By contrast, the concave shape shown in Fig. 10 produces the anticipated compressive deceleration, which is also depicted in Fig. 11.

The effect of a slope discontinuity is indicated in Fig. 12. It is evident that the numerical method accurately locates the initiation of the sonic line at the point (1,0) where the flow is "tripped" to criticality by the acceleration singularity at this location. In most other respects, the pressure distribution is similar to that for Case 1.

In Fig. 13, the effect of a reflex curvature in accelerating the recompression process is shown. As related to comparable turning and wall deflection treated in Case 1, the strength of the terminating shock is considerably increased as well as the magnitude of the pressures near the trailing edge.

The effect of mixed flow conditions at the exit is shown in Figs. 14-16. Here, the function H as well as $\Phi(0,Y)$, comprise the Cauchy data needed to properly pose the hyperbolic portion of the initial manifold. Since the vertical velocity $\Phi_Y(0,Y)$ can be derived as a tangential differentiation, the Cauchy data connotes specification of the additional velocity component for supersonic portions of the jet exit station. Figure 16 indicates that in addition to the usual terminating shock, the transition from hyperbolic to elliptic flow occurs across a weak shock emanating from the specified u discontinuity at (0,1/2).

In Fig. 17, the behavior of centerline pressures for various free jet cases is shown. The monotone subcritical behavior exhibited by these nonlinear cases has not yet been corroborated by rigorous proof based on the boundary value problem with subsonic exit and downstream conditions. For linearized subsonic flow, this property is obvious from the maximum modulus theorem. It should be noted that in the free jet problem discussed here, specified mass flow, pressure ratio and final Mach number M_∞ uniquely determine δ--the scale parameter for the jet displacement.

As a validation, a comparison of numerical and Prandtl-Glauert free jet solutions for u(x,1/2) for $H = 0.35$ and $K = 10$ is shown in Fig. 18, where the analytical solution obtained either from summed eigenfunction expansions or transforms is:

$$u = \frac{2H}{\pi} \tan^{-1} \frac{\sin y^{\dagger}}{\sinh x^{\dagger}} \tag{8a}$$

$$v = -\frac{H\sqrt{K}}{\pi} \ell n \frac{\cosh x^{\dagger} + \cos y^{\dagger}}{\cosh x^{\dagger} - \cos y^{\dagger}} \tag{8b}$$

and

$$x^{\dagger} \equiv \pi x/\sqrt{K} \quad , \quad y^{\dagger} \equiv \pi Y \quad .$$

The slight discrepancies shown in Fig. 18 presumably derive from the small nonlinear effect associated with the finite K value, and truncation errors of the discretizations which are only approximately second order for a non-uniform elliptic mesh. The associated universal slip line curve is obtained from the following integral of (8b)

$$\frac{G_1(x)}{HK} = \frac{1}{2} - \frac{4}{\pi^2}\left\{\sum_0^{\infty} \frac{[1 + x(2n+1)]e^{-(2n+1)x}}{(2n+1)^2} - \frac{x}{2}\,\mathrm{ctnh}^{-1}(\cosh x)\right\} \tag{9}$$

where the daggers have been dropped. Equation (9) has the following limiting behavior

$$\frac{G_1(x)}{HK} = \frac{2}{\pi^2}\left\{-x\ell nx + \left(\frac{1}{2}\ell n4 + 1\right)x + O(x^2)\right\} \quad \text{as } x \to 0$$

$$\frac{G_1(x)}{HK} = \frac{1}{2} - \frac{4}{\pi^2} e^{-x} + O(xe^{-2x}) \quad \text{as } x \to \infty$$

and is plotted in Fig. 19. The asymptotic half width thus checks that given by (8) when the nonlinear second term in the integral is omitted.

Conclusions

Submerged inviscid transonic wall jets have been treated for subsonic conditions infinitely far downstream for a specified exit velocity profile. Unchoked flow has been assumed and a series of wall shapes have been considered giving rise to the following observations:

- Line relaxation provides an efficient means to treat the diversity of wave patterns that can occur, particularly for mixed initial conditions. Accordingly, inverse problems in which contours are identified to reduce wave drag and enhance thrust recovery may represent a feasible near-term possibility.
- A Kutta condition can be satisfied merely by requiring continuity of the potential across the trailing edge. The numerical solution tracks a local singular solution which has a square root zero and is locally harmonic in scaled variables.
- As compared to unconfined flows, the slip line boundaries create a rapid decay of the disturbances. The functional form of the far

field perturbation potential is an exponentially damped sine similar to incompressible flow but different in that its amplitude interacts nonlinearly with the near field.

- Analysis of the free jet case indicates subcritical monotone streamwise variations of the pressure for a subsonic jet exit, as in linear subsonic flow.

- Acceleration of the wall jet to criticality over convex walls is accomplished by stream tube contractions and throats induced by upstream influence of the turning.

- The upper slip line of the wall jet becomes asymptotically parallel to that emanating from the trailing edge infinitely far downstream.

Acknowledgements

This effort was sponsored by the Office of Naval Research under Contract No. N00014-76-C-0350. The authors wish to acknowledge the valuable comments of J. D. Cole and the assistance of J. C. Gysbers with the computational plots.

References

[1] Bevilaqua, P. M. and McCullough, J. K., "Entrainment Method for V/STOL Ejector Analysis," AIAA Paper 76-419, July 1976.

[2] Frankl, F. I., "On the Problem of Chaplygin for Mixed Subsonic and Supersonic Flows," NACA Technical Memorandum TM 1155, 1947.

[3] Chaplygin, S. A., "On Gas Jets," NACA Technical Memorandum, TM 1063, 1944.

[4] Guderley, K. G., The Theory of Transonic Flow, Pergamon Press, Oxford, 1962, pp. 124-127.

[5] Courant, R., and Hilbert, D., Methods of Mathematical Physics, Vol. II, Interscience Publishers, N. Y., pp. 225-226.

[6] Weinstein, A., "Conformal Representation and Hydrodynamics," Proc. First Canadian Math. Congress, University of Toronto Press, Toronto (1946), pp. 355-364.

[7] Murman, E. M., "Analysis of Embedded Shock Waves Calculated by Relaxation Methods," Proc. Computational Fluid Dynamics Conference, Palm Springs, Calif., July 19-20, 1973, pp. 27-40.

[8] Jameson, A., "Iterative Solution of Transonic Flows over Airfoils and Wings, Including Flows at Mach 1," Comm. Pure Appl. Math. 27, 1974, pp. 283-309.

[9] Bailey, F. R. and Ballhaus, W. F., "Comparisons of Computed and Experimental Pressures for Transonic Flows About Isolated Wings and Wing-Fuselage Configurations," in Proc. Conference on Aerodynamic Analyses Requiring Advanced Computers, Part II, Langley Research Center, Hampton, Va, NASA SP-347, March 4-6, 1975, pp. 1213-1232.

[10] Murman, E. M. and Cole, J. D., "Calculations of Plane Steady Transonic Flows," AIAA J. 9, January, 1971, pp. 114-121.

[11] Krupp, J. A., "The Numerical Calculation of Plane Steady Transonic Flows Past Thin Lifting Airfoils," PhD Thesis, University of Washington, Seattle, Wash., June 1971.

[12] Woods, L. C., "The Relaxation Treatment of Singular Points in Poisson's Equation," Quart. J. Mech. and Appl. Math. VI pt. 2, 1953, pp. 163-185.

[13] Murman, E. M., "Computation of Wall Effects in Ventilated Transonic Wind Tunnels," AIAA Paper 72-1007, September 1972.

[14] Pinzola, M. and Lo, C. F., "Boundary Interference at Subsonic Speeds in Wind Tunnels with Ventilated Walls," AEDC Technical Report TR-69-47, May 1969.

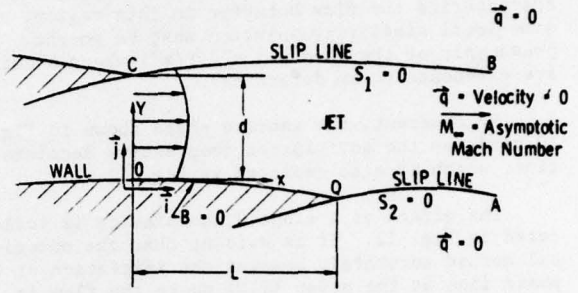

Fig. 1 Wall jet configuration.

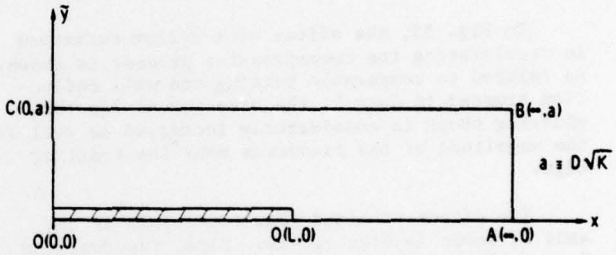

Fig. 2 Transformed wall jet domain.

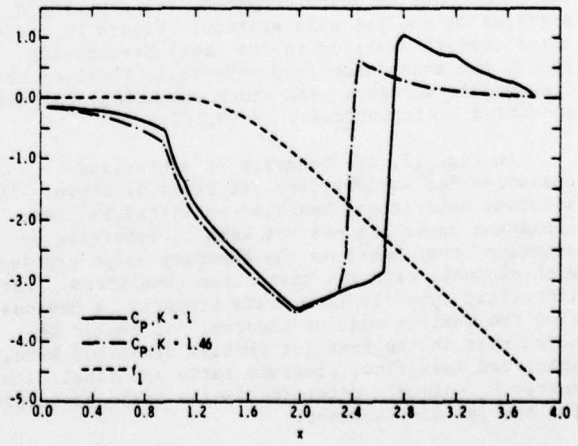

Fig. 3 Pressures along wall for K = 1 and K = 1.46, f_1 = normalized wall ordinate.

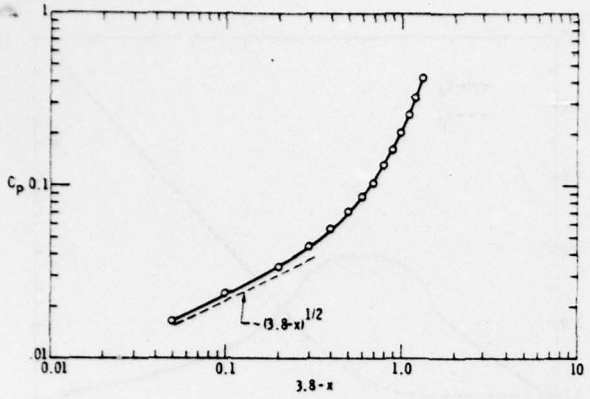

Fig. 4 Local solution near trailing edge, Case 1.

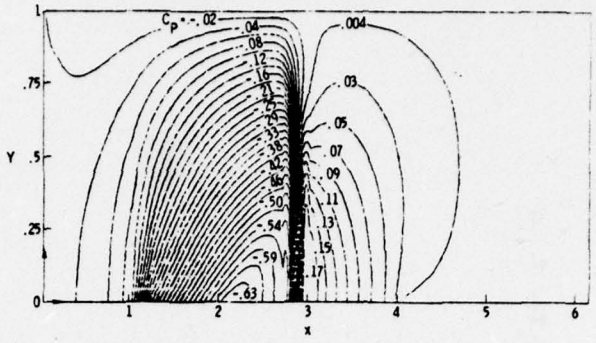

Fig. 5 Isobars for Case 1.

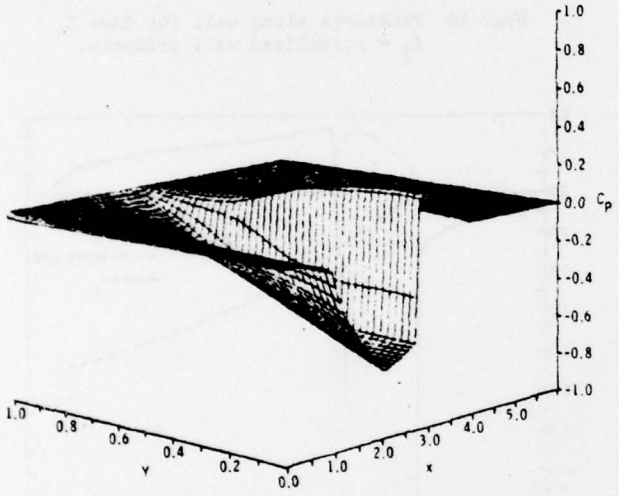

Fig. 6 C_p surface for Case 1.

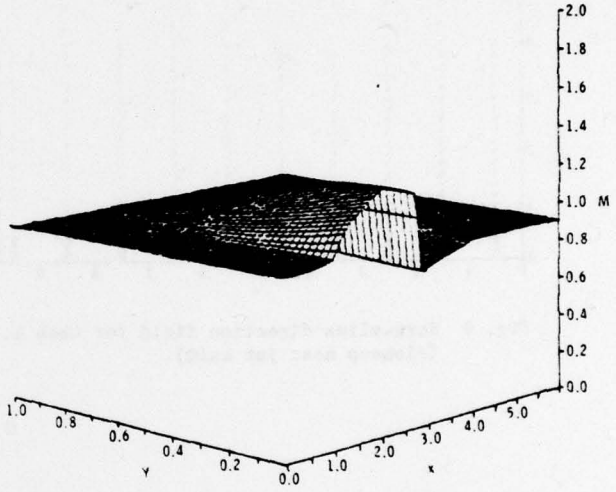

Fig. 7 Mach surface for Case 1.

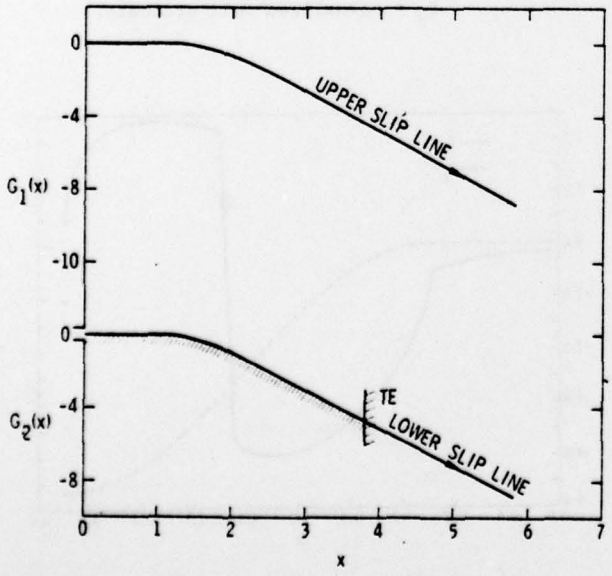

Fig. 8a Slip line shapes for Case 1.

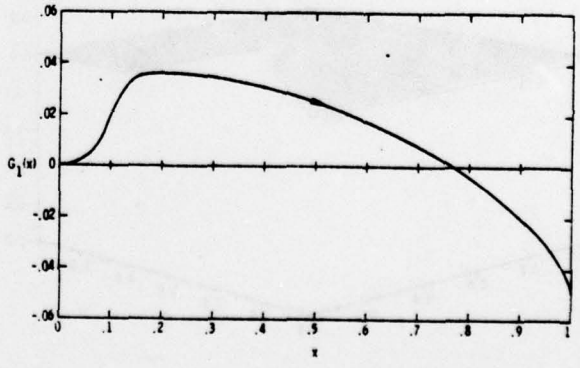

Fig. 8b Closeup of slip lines near jet exit for Case 1.

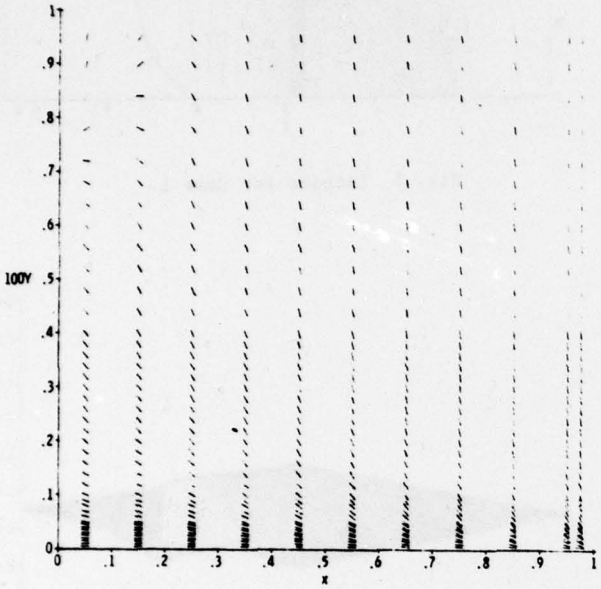

Fig. 9 Streamline direction field for Case 1, (closeup near jet exit).

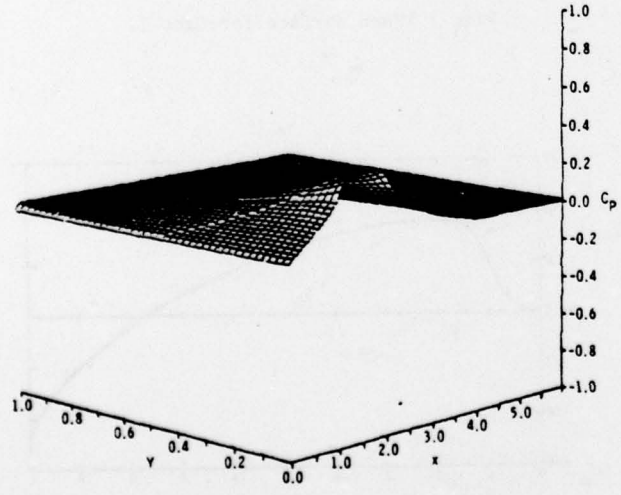

Fig. 11 Pressure surface for Case 2.

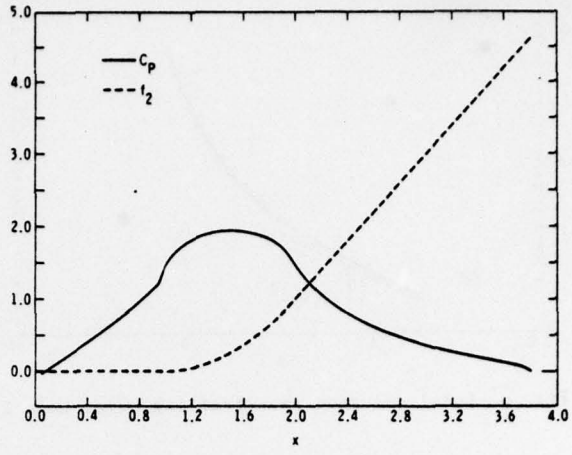

Fig. 10 Pressures along wall for Case 2, f_2 = normalized wall ordinate.

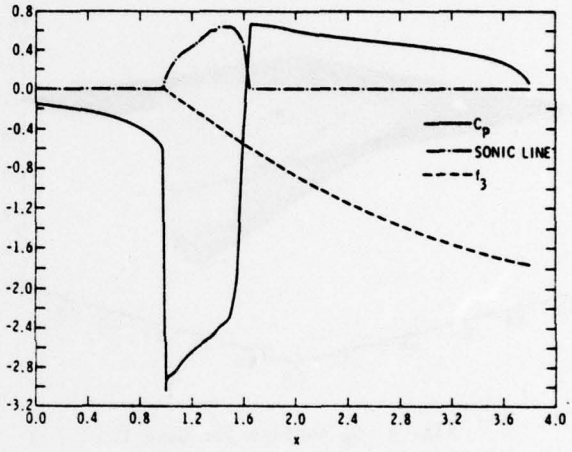

Fig. 12 Pressures along wall for Case 3, f_3 = normalized wall ordinate.

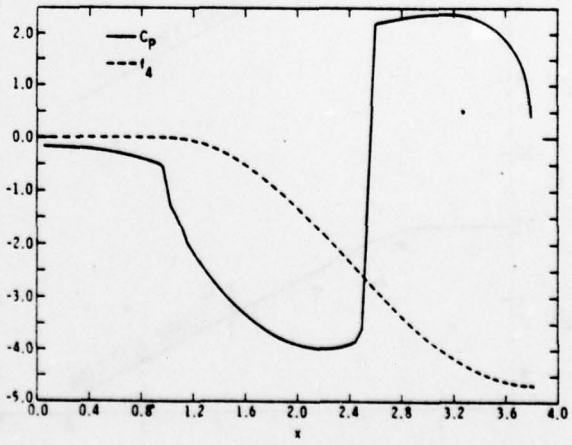

Fig. 13 Pressures along wall for Case 4, f_4 = normalized wall ordinate.

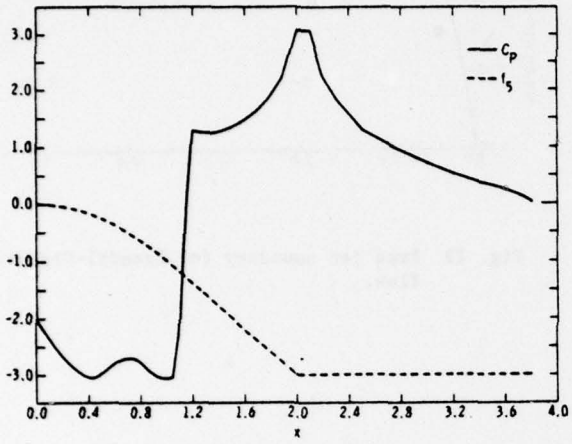

Fig. 14 Pressures along wall for Case 5 (partially supersonic jet exit), f_5 = normalized wall ordinate.

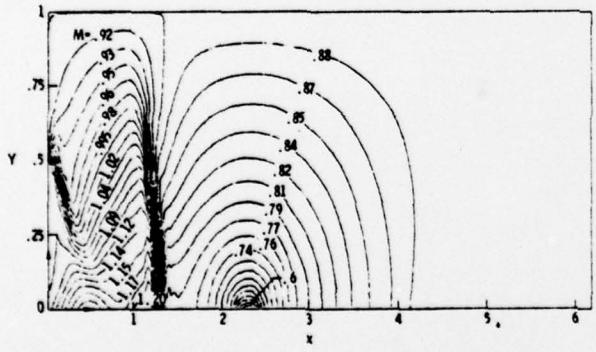

Fig. 16 Mach contours for Case 5.

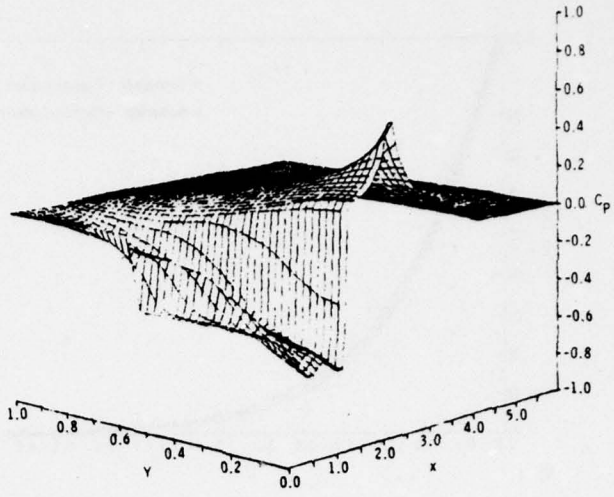

Fig. 15 Pressure surface for Case 5.

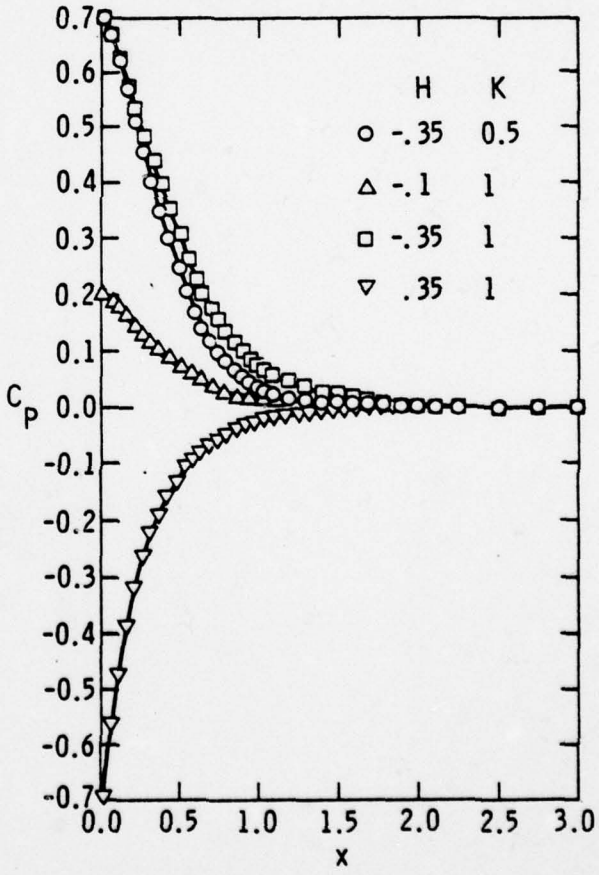

Fig. 17 Centerline pressures for a transonic free jet for various pressure ratios and similarity parameters, K.

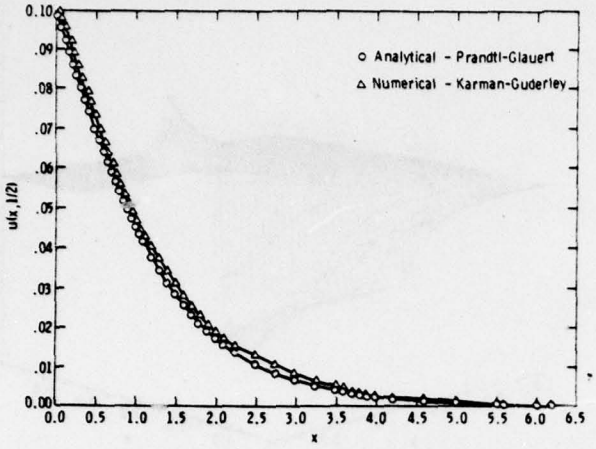

Fig. 18 Comparison of free jet analytical and numerical solutions.

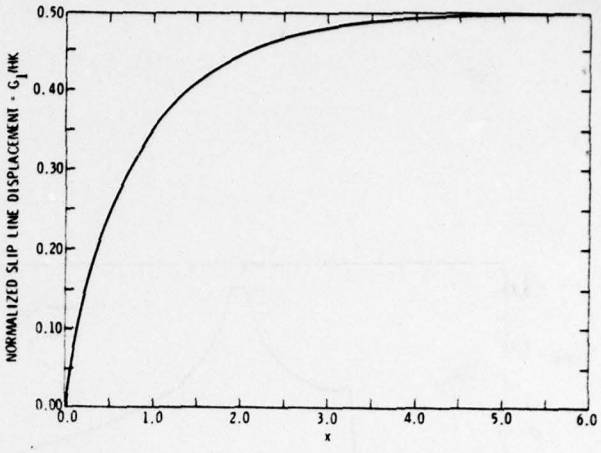

Fig. 19 Free jet boundary for Prandtl-Glauert flow.

UNCLASSIFIED

SECURITY CLASSIFICATION OF THIS PAGE (When Date Entered)

REPORT DOCUMENTATION PAGE

READ INSTRUCTIONS BEFORE COMPLETING FORM

1. REPORT NUMBER

2. GOVT ACCESSION NO.

3. RECIPIENT'S CATALOG NUMBER

4. TITLE (and Subtitle)

AN INVISCID MODEL FOR SUBMERGED TRANSONIC WALL JETS

5. TYPE OF REPORT & PERIOD COVERED

Reprint/ AIAA Paper 77-174

6. PERFORMING ORG. REPORT NUMBER

SC-PP-76-124

7. AUTHOR(s)

W. D. Malmuth and W. D. Murphy

8. CONTRACT OR GRANT NUMBER(s)

N00014-76-C-0350

9. PERFORMING ORGANIZATION NAME AND ADDRESS

Rockwell International Corporation
Science Center
1049 Camino Dos Rios, P.O. Box 1085
Thousand Oaks, CA 91360

10. PROGRAM ELEMENT, PROJECT, TASK AREA & WORK UNIT NUMBERS

NR 061-234 (438)

11. CONTROLLING OFFICE NAME AND ADDRESS

Office of Naval Research
Department of the Navy
300 N. Quincy St.
Arlington, VA 22217

12. REPORT DATE

December 1976

13. NUMBER OF PAGES

12

14. MONITORING AGENCY NAME & ADDRESS (if different from Controlling Office)

AFPRO, Rockwell International Corporation
B-1 Division
Los Angeles International Airport
Los Angeles, CA 90009

15. SECURITY CLASS. (of this report)

Unclassified

15a. DECLASSIFICATION/DOWNGRADING SCHEDULE

16. DISTRIBUTION STATEMENT (of this Report)

Approved for public release; distribution unlimited

17. DISTRIBUTION STATEMENT (of the abstract entered in Block 20, if different from Report)

18. SUPPLEMENTARY NOTES

19. KEY WORDS (Continue on reverse side if necessary and identify by block number)

TRANSONIC FLOW, JETS LIFT, PROPULSION SYSTEMS, SHOCK WAVES, EJECTORS, AUGMENTOR WINGS, FLAPS (CONTROL SURFACES)

20. ABSTRACT (Continue on reverse side if necessary and identify by block number)

Nonlinear flow phenomena in transonic wall jets prototypic of propulsive lift devices such as lifting ejector augmenters and upper surface blown wings have been studied using the Karman-Guderley model. From modern line relaxation methods, an efficient computational method has been developed to treat the diversity of shock patterns produced by various wall shapes and exit conditions. Associated with the algorithm is a far field determined analytically from the boundary value problem appropriate to subsonic conditions far downstream. Numerical results for circular arc boattails indicate rapid relaxation of the wall induced distrubances, and

DD FORM 1 JAN 73 1473 EDITION OF 1 NOV 65 IS OBSOLETE

Unclassified

SECURITY CLASSIFICATION OF THIS PAGE (When Date Entered)

389 949

in the supersonic region. Partially subsonic and supersonic jet exit conditions lead to the anticipated wave interactions. Studies of other shapes show that branch point singular behavior associated with satisfaction of a Kutta condition at the wall trailing edge is obtained by demanding continuity of the perturbation potential at this point.